Deep water provenance and dynamics of the (de)glacial Atlantic meridional overturning circulation

Jörg Lippold, Marcus Gutjahr, Patrick Blaser, Emanuel Christner, Maria Luiza de Carvalho Ferreira, Stefan Mulitza, Marcus Christl, Frank Wombacher, Evelyn Böhm, Benny Antz, et al.

Deep water provenance and dynamics of the (de)glacial Atlantic meridional overturning circulation

Jörg Lippold[1,2*], Marcus Gutjahr[3,4], Patrick Blaser[2], Emanuel Christner[2], Maria Luiza de Carvalho Ferreira[2], Stefan Mulitza[5], Marcus Christl[6], Frank Wombacher[7,8], Evelyn Böhm[2,9], Benny Antz[2], Olivier Cartapanis[1], Hendrik Vogel[1], Samuel L. Jaccard[1]

[1]Institute of Geological Sciences and Oeschger Centre for Climate Change Research, University of Bern, 3012 Bern, Switzerland.

[2] Institute of Environmental Physics, University of Heidelberg, 69120 Heidelberg, Germany.

[3] Bristol Isotope Group, Department of Earth Sciences, Wills Memorial Building, Bristol BS8 1RJ, UK.

[4] GEOMAR Helmholtz Centre for Ocean Research Kiel, 24148 Kiel, Germany.

[5] MARUM - Center for Marine Environmental Sciences, University of Bremen, 28359 Bremen, Germany.

[6] ETH Zurich, Laboratory of Ion Beam Physics, 8093 Zurich, Switzerland.

[7] Institut für Geologie und Mineralogie, Universität zu Köln, 50674 Köln, Germany.

[8] Steinmann Institut, Universität Bonn, 53115 Bonn, Germany.

[9] LSCE, Gif-Sur-Yvette, France.

[*]corresponding author: joerg.lippold@geo.unibe.ch

Keywords: $^{231}Pa/^{230}Th$; ε_{Nd}; Atlantic Meridional Overturning Circulation; deep sea sediments; Last Glacial Maximum; deglaciation

Abstract

Reconstructing past modes of ocean circulation is an essential task in paleoclimatology and paleoceanography. To this end, we combine two sedimentary proxies, Nd isotopes (ε_{Nd}) and the $^{231}Pa/^{230}Th$ ratio, both of which are not directly involved in the global carbon cycle, but allow the reconstruction of water mass provenance and provide information about the past strength of overturning circulation, respectively. In this study, combined $^{231}Pa/^{230}Th$ and ε_{Nd} down-core profiles from six Atlantic Ocean sediment cores are presented. The data set is complemented by the two available combined data sets from the literature. From this we derive a comprehensive picture of spatial and temporal patterns and the dynamic changes of the Atlantic Meridional Overturning Circulation over the past ~ 25 ka. Our results provide evidence for a consistent pattern of glacial/stadial advances of Southern Sourced Water along with a northward circulation mode for all cores in the deeper (> 3,000 m) Atlantic. Results

from shallower core sites support an active overturning cell of shoaled Northern Sourced Water during the LGM and the subsequent deglaciation. Furthermore, we report evidence for a short-lived period of intensified AMOC in the early Holocene.

1 Introduction

Today, the Atlantic Meridional Overturning Circulation (AMOC) accounts for ~50 % of the planetary poleward advection of heat and contributes to the removal of CO_2 from the surface ocean through the formation of nutrient-depleted North Atlantic Deep Water (NADW) (Sabine et al., 2004). A change in the relative volumetric contribution of North Atlantic- versus Southern Ocean-sourced waters during the last deglaciation is considered to have significantly impacted the efficiency of the marine soft tissue pump and associated alkalinity feedbacks, thereby directly altering the partitioning of CO_2 between the ocean interior and the atmosphere (Jaccard et al., 2016).

Studies using the non-conservative nutrient-tracers $\delta^{13}C$ and Cd/Ca in benthic foraminifera or radiocarbon ventilation ages have provided a wealth of evidence that the water mass distribution in the glacial North Atlantic was significantly different from the modern geometry (e.g. (Curry and Oppo, 2005)). Today NADW occupies most of the water column in the western North Atlantic. During the Last Glacial Maximum (LGM) waters below about 2,500 to 3,000 m were dominated by nutrient-rich deep waters likely originating from the Southern Ocean (Southern Component Water, SCW), while the upper limb was bathed by a relatively fresher water mass referred to as Glacial North Atlantic Intermediate Water (GNAIW) (Lynch-Stieglitz and Fairbanks, 1994). During the deglaciation the GNAIW depth distribution evolved into the modern situation of NADW, dominating the North Atlantic down to ~5,000 m water depth. However, reconstruction of the exact spatial and temporal sequence of events characterising deglacial AMOC mode changes is not straightforward and remains a matter of debate.

Our current understanding of the glacial, deglacial and Holocene evolution of Atlantic Ocean circulation patterns is mainly based on paleoceanographic reconstructions gleaned from carbon isotopes, in particular benthic foraminifera $\delta^{13}C$. While benthic foraminifera-derived $\delta^{13}C$ provide useful information about the geometry of subsurface circulation patterns, it only provides incomplete constraints about flow rates. Furthermore, the benthic $\delta^{13}C$ signal is influenced by a number of factors, complicating its interpretation. The average $\delta^{13}C$ of the global ocean is a function of changes in the amount of carbon stored on land and is affected by changes in the sinks and sources of carbon reservoirs. Furthermore, $\delta^{13}C$ may be sensitive to the balance of photosynthesis versus respiration, microhabitat conditions and CO_2 air-sea gas exchange, because the equilibration timescale in the surface ocean is proportional to the ratio of dissolved inorganic carbon to CO_2 (Galbraith et al., 2015).

Seawater-derived $^{231}Pa/^{230}Th$ and Nd isotopes provide two independent, yet complementary proxies of past ocean circulation, which are insensitive to variations in the global carbon cycle. While the first proxy, based on the sedimentary distribution of protactinium/thorium isotopes ($^{231}Pa/^{230}Th$), provides quantitative information about the strength and the dynamics of overturning circulation (McManus et al., 2004), the second proxy, based on the authigenic neodymium isotopic composition ($^{143}Nd/^{144}Nd$), allows the fingerprinting of water mass provenance and therefore constraining flow paths throughout the deep ocean (e.g. Frank, 2002; Piotrowski et al., 2004).

Although, the spatial and temporal coverage of ε_{Nd} and $^{231}Pa/^{230}Th$ data sets from the last glacial cycle is continuously improving, the lack of direct comparison between circulation strength-, water mass provenance- and nutrient- proxies still does not provide a consistent picture of glacial and deglacial AMOC changes. There is a coherent picture of a glacial deep Atlantic dominated by SCW, which was gradually replaced by NCW during the deglacial and the Holocene (e.g. (Gutjahr et al., 2008; Piotrowski et al., 2004)) indicated by Nd-isotope signatures in agreement with findings based on carbon isotopes (e.g. (Curry and Oppo, 2005; Sarnthein et al., 1994)). Compilations of $^{231}Pa/^{230}Th$ data sets (Bradtmiller et al., 2014; Gherardi et al., 2009; Lippold et al., 2012b) found generally higher values in the deep Atlantic and unchanged or lower values in shallower waters compared to the Holocene. These studies suggest that the shallower circulation cell exhibited stronger overturning than the deeper cell during the LGM and are also consistent with the interpretation of a still active but reduced net ocean overturning during Heinrich Stadial 1 (HS1). The first publication presenting combined $^{231}Pa/^{230}Th$ (McManus et al., 2004) and ε_{Nd} (Roberts et al., 2010) from two neighbouring sediment cores from the Bermuda Rise (GGC5 and GGC6) revealed a high degree of synchronicity between the changes in water mass provenance and circulation strength across the last glacial termination. More recently this approach was extended, in another adjacent Bermuda Rise sediment core from a similar water depth (ODP1063, Table 1), covering the last 140 ka (Böhm et al., 2015). These studies found a gradual transition from a SCW dominated deep North-West Atlantic during the LGM into a Northern Component Water (NCW) dominated vigorous circulation state. This active circulation prevailed for most of the last glacial cycle with a continuous strong contribution of NCW in the deep Atlantic as indicated from Nd isotope signatures, while the domination of sluggishly ventilated SCW was restricted to time ranges around the peak glacial. Although temporaly highly resolved, these reconstructions were derived from a single location and thus may be subject to local obfuscating factors. Here we present combined measurements of $^{231}Pa/^{230}Th$ and $^{143}Nd/^{144}Nd$ from two published and six new data sets, spanning a latitudinal transect across the entire Atlantic, to infer past changes in both the strength and geometry of the AMOC back to the LGM. Particular attention is paid to consistencies and discrepancies between the combined proxy records and the presence or absence of gradients between neighbouring core sites. Our results thus aim to provide an updated illustration of the potential of this combined multi-core $^{231}Pa/^{230}Th$ and ε_{Nd} isotope approach.

2 Materials and methods

2.1 Overview of core locations, measurements and age controls

The eight sediment core locations cover a meridional transect through the North and South Atlantic Ocean with a wide range of water depths and hydrological settings from 42°N to 40°S (Table 1). The six new combined profiles are measured from sediment cores featuring well-established, published age models (supplementary material, S4), with the exception of GeoB1523-1, for which a chronology was determined by comparison of its down-core $\delta^{18}O$ record to the adjacent ^{14}C dated core GeoB1515-1 (Vidal et al., 1999). Results are provided in the supplementary material (Table S6). Two locations from the literature with combined $^{231}Pa/^{230}Th$ and ε_{Nd} down-core profiles complement the compilation: GeoB3808-6 from the South Atlantic (Jonkers et al., 2015) and a high-resolution composite from the Bermuda Rise based on records from three adjacent sediment cores (GGC5: (McManus et al., 2004), GGC6: (Roberts et al., 2010) and ODP1063: (Lippold et al., 2009), (Gutjahr and Lippold, 2011)).

a

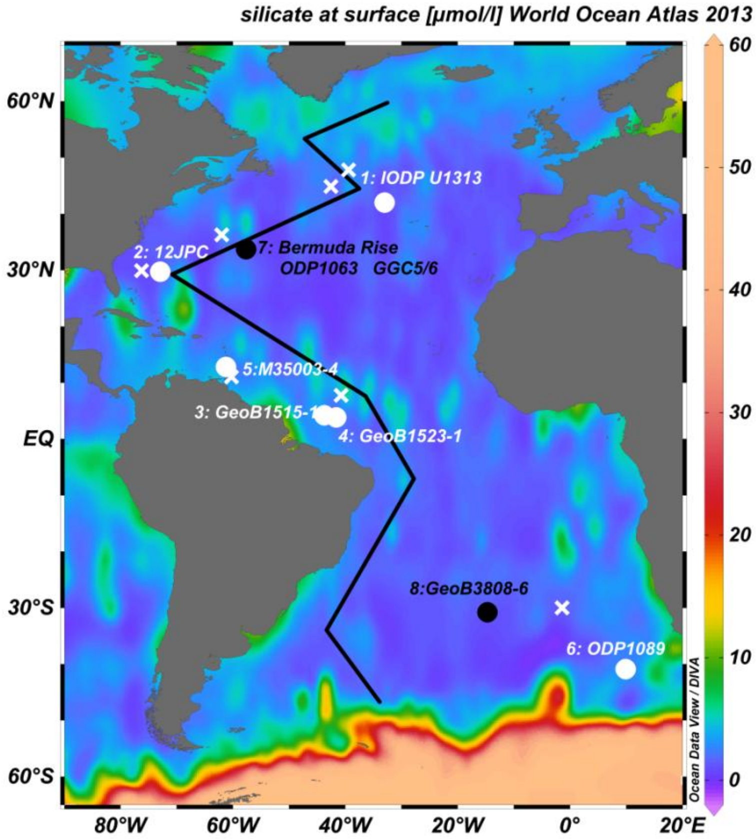

b

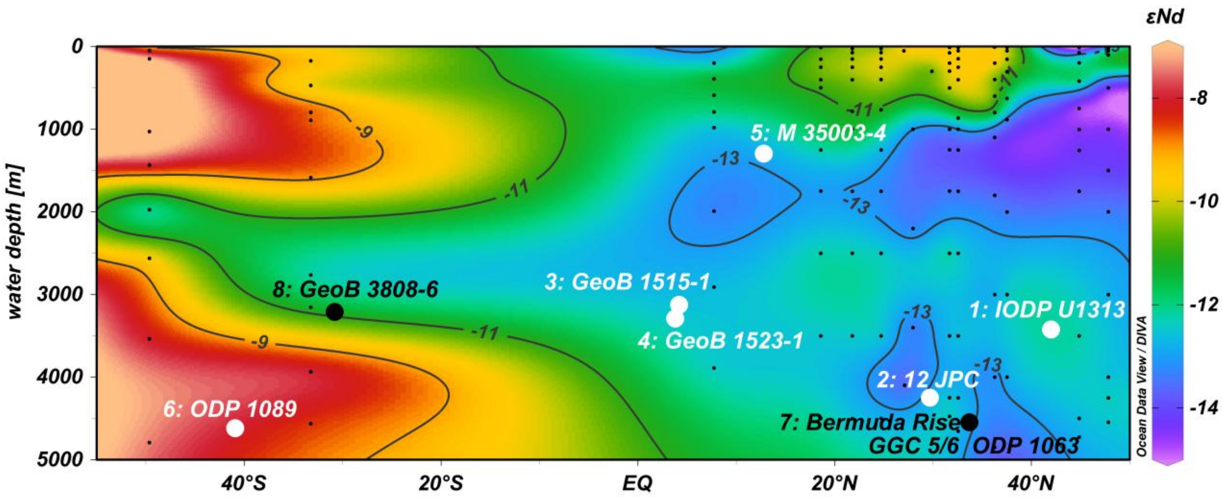

Fig. 1: (a) Core locations (new data: white, literature data: black) overlain by surface silicate concentrations from World Ocean Atlas 2013. The black line tracks the section of water stations used for Fig.1b. White crosses indicate locations of nearest water stations with seawater measurements of Nd isotopes (see supplementary material S2).

(b) A longitudinal section showing the core locations and published ε_{Nd} in seawater from the West-Atlantic Ocean (black dots) (Jeandel, 1993; Lambelet et al., 2015; Osborne et al., 2014;

Piepgras and Wasserburg, 1987) highlighting the distinct Nd isotope compositions of NCW and SCW.

Table 1: Overview of measurements and age models of sediment cores with combined $^{231}Pa/^{230}Th$ and ε_{Nd} data sets including the published data sets from the Bermuda Rise (ODP1063 and GGC5/6) and the South Atlantic (GeoB3808-6). Further information on the age models is provided in the supplementary material S4.

core number in figures		**water depth [m]**	**lat. N**	**long. E**	ε_{Nd}	**Pa/Th**
	this study					
1	**IODP Site U1313**	3426	41.0	-33.0	this study	this study
2	**12JPC**	4250	29.7	-72.9	(Gutjahr et al., 2008)	this study and (Lippold et al., 2012b) (Holocene and LGM time slices)
3	**GeoB1515-1**	3129	4.2	-43.7	this study	this study and (Lippold et al., 2011; Lippold et al., 2012b) (Holocene and LGM time slices)
4	**GeoB1523-1**	3292	3.8	-41.6	this study	this study and (Lippold et al., 2011; Lippold et al., 2012b) (Holocene and LGM time slices)
5	**M35003-4**	1299	12.1	-61.2	this study	this study and (Lippold et al., 2012b) (Holocene and LGM time slices)
6	**ODP Site 1089**	4621	-40.9	9.9	this study	this study and (Lippold et al., 2012a) (Holocene and LGM time slices
	literature data					
7	**ODP Site 1063**	4584	33.7	-57.6	(Böhm et al., 2015; Gutjahr and Lippold, 2011)	(Böhm et al., 2015; Lippold et al., 2009)
7	**GGC5/GGC6**	4550	33.7	-57.6	(Roberts et al., 2010)	(McManus et al., 2004)
8	**GeoB3808-6**	3213	-30.8	-14.7	(Jonkers et al., 2015)	(Jonkers et al., 2015)

2.2 Neodymium isotopes

In recent years the measurement of Nd isotopes on sub-millennial timescales has been developed and applied using bulk sediment leachates, foraminifera coatings, deep-sea corals and fish teeth (e.g. (Colin et al., 2010; Elmore et al., 2011; Gutjahr et al., 2008; Pahnke et al., 2008; Piotrowski et al., 2004; Roberts et al., 2010)). The rationale for using Nd isotopes as a water mass provenance tracer is based on the empirical observation that large parts of northern North America bordering the Labrador Sea consist of Archean and Proterozoic continental crust featuring low (unradiogenic) $^{143}Nd/^{144}Nd$ ratios, whereas young mantle-derived rocks display high (radiogenic) isotopic compositions. For convenience, the radiogenic Nd isotope ratio $^{143}Nd/^{144}Nd$ is expressed as the deviation from a chondritic uniform reservoir (CHUR) in epsilon (ε) notation:

$$\varepsilon_{Nd} = \left[\frac{^{143}Nd/^{144}Nd_{sample}}{^{143}Nd/^{144}Nd_{CHUR}} - 1 \right] \times 10^4$$

Neodymium is dominantly supplied to the oceans through weathering of continental crust or boundary exchange along continental margins. Labrador Sea Water (LSW) is characterised by a very distinct unradiogenic Nd isotopic composition ($\varepsilon_{Nd} \approx -14$) (Lacan and Jeandel, 2005a; Piepgras and Wasserburg, 1987). LSW is admixed to the Deep Western Boundary Current (DWBC) to form North Atlantic Deep Water (NADW). While NADW is characterised by unradiogenic values, SCW is characterised by a consistently more radiogenic Nd isotopic composition ($\varepsilon_{Nd} \approx -8$ today) due to the admixture of radiogenic Pacific waters ($\varepsilon_{Nd} \approx -4$) in the Antarctic Circumpolar Current. In the open ocean Nd behaves semi-conservatively with a residence time between ~500 and 2000 years, making it an ideal proxy to trace water mass exchange between the major ocean basins (Frank, 2002).

Neodymium is enriched in the authigenic Fe-Mn oxyhydroxide fraction of marine sediments. This fraction records the dissolved Nd isotope composition of the sediment-bottom water interface (Gutjahr et al., 2007; Piotrowski et al., 2004). For this study, the isotope composition of authigenic Nd was derived from bulk sediment leachates and applied as a palaeo-water mass proxy. This approach, however, has some limitations which need to be considered carefully (e.g. Elmore et al. 2011). Firstly, boundary exchange is an efficient mechanism to alter the ε_{Nd} of bottom water along ocean margins (Lacan and Jeandel, 2005b). However, the consistent north-south gradient of ε_{Nd} in Atlantic waters, observable for marginal locations, implies that local boundary exchange does not affect the first-order spatial distribution of dissolved Nd. However, in order to minimise potential bias on ε_{Nd} it is recommended to examine the authigenic Fe-Mn oxyhydroxide fraction of marine sediments from locations where ocean water is well mixed. Another source of uncertainty may arise from non-selective leaching of volcanic ash in the sediments. At locations in the vicinity of Iceland ε_{Nd} values have been reported to be different from seawater composition. All sediment cores used in this study are located outside these areas of potential ash contamination (Elmore et al., 2011). Nonethelss, the reliablitiy of our leaching method has been tested by comparing the ε_{Nd} from the youngest available Holocene sample leachate to the water-derived ε_{Nd} from the closest available water cloumn station (supplementary material, S2).

Sample preparation and measurement

The method applied here follows the procedure outlined by Gutjahr et al. (2007). Briefly, approximately 0.25 g of ground bulk sediment was first leached with $MgCl_2$ in order to remove loosely adsorbed metals. Subsequently, the sediment was decarbonated with buffered acetic acid and finally the authigenic metal oxyhydroxide fraction was extracted with a reductive cocktail containing 0.03 M EDTA, 0.05 M hydroxylamine-hydrochloride and 15% acetic acid, buffered to a pH of 4 using NaOH. The Fe-Mn oxyhydroxide leaching step was carried out at room temperature for 2 hours under constant agitation. The leachate was decanted after centrifugation and subsequently purified for isotope analysis. The purification by column chemistry followed standard procedures as described in Böhm et al. (2015). The Rare Earth Elements (REE) were first separated from the bulk matrix using 50W-X8 resin and after conversion to nitrate Nd is separated from the other REE with LN spec resin. Our Nd isotope measurements were performed on two Thermo Finnigan Neptune multiple collector inductively coupled plasma mass spectrometers (ICP-MS) at the University of Bristol (UK) and the National Oceanography Centre Southampton (UK). Instrumental mass discrimination was corrected relative to $^{146}Nd/^{144}Nd = 0.7219$ using the mass bias correction procedure of Vance and Thirlwall (2002). All Nd isotope compositions were normalised to $^{143}Nd/^{144}Nd = 0.512115$ for the JNdi-1 standard (Tanaka et al., 2000). External reproducibility of the $^{143}Nd/^{144}Nd$ based on repeated standard measurements amounted to 0.20 ε_{Nd}. Results are given in the supplementary data table S3.

2.3 $^{231}Pa/^{230}Th$ as a kinematic circulation proxy

The radioisotopes ^{231}Pa ($t_{½}$: 32.5 ka) and ^{230}Th ($t_{½}$: 75.2 ka) are formed by alpha decay of natural ^{235}U and ^{234}U, respectively, at a constant activity ratio of 0.093, globally. While U is soluble, Pa and Th are highly particle reactive and are thus readily scavenged from seawater by sinking particles resulting in the accumulation of excess- or unsupported ^{230}Th and ^{231}Pa in underlying sediments (i.e. $^{231}Pa/^{230}Th_{xs}$, termed $^{231}Pa/^{230}Th$ thereafter). ^{231}Pa is however less rapidly removed than ^{230}Th and has a residence time approaching the transit time of deep water in the Atlantic basin. As a result, approximately half of the ^{231}Pa produced in Atlantic water is exported along with North Atlantic Deep Water into the Southern Ocean instead of being buried in Atlantic sediments. Hence, ^{231}Pa/^{230}Th from modern north Atlantic core-top sediments displays values below the production ratio, reflecting a deficit of ^{231}Pa as a consequence of the net export by NADW to the Southern Ocean (McManus et al., 2004). However, sedimentary ^{231}Pa/^{230}Th is not only a function of circulation strength and geometry, but may also be affected by particle composition - with biogenic opal preferentially scavenging ^{231}Pa (Chase et al., 2002) -, particle size (Kretschmer et al., 2008), particle flux (Christl et al., 2010) and water depth (Gherardi et al., 2009; Lippold et al., 2011; Scholten et al., 2008). Sediments from shallower waters of the North Atlantic are characterised by high ^{231}Pa/^{230}Th because a strong circulation regime produces high ^{231}Pa/^{230}Th, as a result of enhanced scavenging of ^{231}Pa close to the surface combined with the downstream ingrowth of ^{231}Pa (Luo et al., 2010). Due to this complex behaviour reconstructions of past AMOC by ^{231}Pa/^{230}Th should include samples from several water depths and latitudes as different modes of AMOC are capable of producing similar sedimentary ^{231}Pa/^{230}Th at different locations (Luo et al., 2010). The interpretation of ^{231}Pa/^{230}Th is further complicated by the fact that ^{231}Pa/^{230}Th may provide information about the export of ^{231}Pa but no information about the direction of this lateral export. Consequently, the application of ε_{Nd} combined with ^{231}Pa/^{230}Th holds promise for reconstructing both past water mass provenance and circulation strength of the Atlantic Ocean.

Pa/Th-sample preparation and measurement

Sedimentary ^{231}Pa-excess was determined by isotope dilution using a ^{233}Pa spike milked from ^{237}Np. A ^{229}Th and a ^{236}U spike were used to determine the concentrations of ^{230}Th, ^{232}Th and ^{238}U with MC-ICP-MS, respectively. The chemical separation and cleaning followed standard procedures (e.g. (Böhm et al., 2015)). The ^{233}Pa spike was calibrated against the reference standard material UREM-11 (Geibert and Vöge, 2008). U, Th and Pa isotopes from cores GeoB1515-1, GeoB1523-1, 12JPC and M35003-4 were measured using a Neptune MC-ICP-MS at the joint Cologne/Bonn mass spectrometer laboratory at the Universität Bonn. The abundance of ^{231}Pa in samples from ODP Site 1089 have been measured using the AMS system TANDY following the method described by Christl et al. (2007), whereas the U and Th fractions were measured using a Neptune MC-ICP-MS. U, Th and Pa isotopes from IODP1313 were measured using the Thermo Finnigan Element 2 ICP-MS at the University of Heidelberg. Data and uncertainties are provided in the supporting material S6.

The measured bulk sediment concentrations of ^{231}Pa and ^{230}Th comprise contributions from the lithogenic (produced by radioactive decay of U present in the mineral lattices) and authigenic fractions (produced by decay of U that was incorporated under reducing conditions), which need to be accounted- and corrected for. The lithogenic contribution was corrected considering a distinct lithogenic ^{238}U/^{232}Th activity ratio for each core location. In several cases a basin-wide lithogenic ^{238}U/^{232}Th in the range of 0.6±0.1 would have led to systematic inaccuracies due to local variations (Bourne et al., 2012). When oxygen concentrations at the sediment-water interface were high enough to prevent authigenic uranium enrichments the bulk ^{238}U/^{232}Th minima were used as an upper limit for the lithogenic correction. Accordingly, for GeoB1515-1 and GeoB1523-1 a $(^{238}U/^{232}Th)_{lith}$ value of 0.47 has been considered. For 12JPC and M35003-4 values of 0.55 and 0.60 have been used, respectively. High bulk ^{238}U/^{232}Th ratios at both IODP Site U1313 and ODP Site 1089 indicate consistent authigenic U enrichment throughout the deglacial interval. Thus, a $(^{238}U/^{232}Th)_{lith}$ value of 0.6 for IODP Site U1313 and ODP Site 1089 respectively has been applied. Further, a disequilibrium of 4% for ^{234}U/^{238}U in the lithogenic fraction has been considered to account for preferential ^{234}U loss via the recoil-effect (Bourne et al., 2012). The selection of $(^{238}U/^{232}Th)_{lith}$ is of subordinate importance for the final ^{231}Pa/^{230}Th ratios, as shown in the supplementary material S3, with the exception of the shallowest core M35003-4. Even for this core the relative variations of ^{231}Pa/^{230}Th are not substantially influenced by the $(^{238}U/^{232}Th)_{lith}$ value.

Biogenic Opal

Since ^{231}Pa shows a higher affinity for biogenic silicate particles (Chase et al., 2002) the sedimentary opal content has been carefully monitored before interpreting ^{231}Pa/^{230}Th in terms of ocean circulation strength (supplementary material, S5). Opal measurements were performed by either automated leaching or by Fourier transformation infrared spectroscopy (FTIRS).

3 Results and discussion

Six new combined ^{231}Pa/^{230}Th and ε_{Nd} down-core profiles represent a considerable improvement in the available data bases of both proxies. We therefore present a short outline of the new results from each core before discussing what can be deduced from a comprehensive compilation of all data sets along with the literature records.

In order to provide support of the applications ^{231}Pa/^{230}Th results are also presented as a function of of opal concentrations in section 3.6. For Nd isotopes the comparison of seawater measurements to late Holocene Fe-Mn oxide leachates provide evidence for the reliability of our bulk sediment leachates in recording a past seawater ε_{Nd} signal. No core top samples could be used for this study, but ε_{Nd} values from the youngest samples (5.5 – 0.1 ka) of each core are in good agreement with the seawater compositions from the closest available stations (supplementary material, S2).

3.1 IODP U1313

The northernmost core location, IODP Site U1313 (3,426 m water depth, (Channell et al., 2006)) displays $^{231}Pa/^{230}Th$ values (n=21) that are always clearly below the production ratio and with relatively low variability throughout the record (min=0.046, max=0.068; Fig. 2a). The variability is much smaller compared with the $^{231}Pa/^{230}Th$ records from the Bermuda Rise, where the prodution ratio of 0.093 was reached during HS1 and HS2 (Lippold et al., 2009; McManus et al., 2004). The values are generally in good agreement with $^{231}Pa/^{230}Th$ data from a shallower adjacent core (MD95-2037 (Gherardi et al., 2009), supporting material S1). There is no pronounced increase during HS1, which may be, however, a result of the low temporal resolution towards the younger part of the record.

The Nd isotope record delineates two distinct levels of more radiogenic glacial values followed by rather unradiogenic ε_{Nd} in the deglacial and the Holocene with a relatively sharp transition at ~ 17 ka. This general trend is similar to the ε_{Nd} records from deep north-west-Atlantic locations (e.g. (Gutjahr et al., 2008; Roberts et al., 2010)), but the onset to less radiogenic values occurs earlier. In contrast to its $^{231}Pa/^{230}Th$ record, the ε_{Nd} of IODP Site U1313 is more similar to the records from the other cores sites of this study (Fig. 2).

3.2 12JPC

We complemented an existing ε_{Nd} profile (Gutjahr et al., 2008) from core 12JPC (4,250 m water depth, (Keigwin, 2004)) with $^{231}Pa/^{230}Th$ measurements (n=18) from the identical sample material (Fig. 2b). The transition from radiogenic Nd isotope signatures during the LGM to more unradiogenic Nd isotopes during the Holocene ($\Delta\varepsilon_{Nd}\approx3$) is also recorded by a shift towards lower $^{231}Pa/^{230}Th$.. The relative gradient in $^{231}Pa/^{230}Th$, however, is less pronounced than the glacial-interglacial gradient in the ε_{Nd} signatures. The gradient between maximum (0.083) and minimum (0.058) $^{231}Pa/^{230}Th$ values is comparable to the gradient observed for IODP U1313. But unlike for IODP Site U1313 the record can be separated into higher glacial ($^{231}Pa/^{230}Th$ average=0.076, n=5) and deglacial (average=0.077, n=8) values, followed by clearly lower Holocene values (average=0.058, n=4) This record is more similar to the deglacial $^{231}Pa/^{230}Th$ profile from Bermuda Rise (McManus et al., 2004), although featuring significantly higher values during the LGM as well as lacking the distinctive $^{231}Pa/^{230}Th$ peak during HS1.

3.3 GeoB1515-1 and GeoB1523-1

In order to evaluate the consistency and variability of the signals recorded by $^{231}Pa/^{230}Th$ and ε_{Nd}, we used sample material from two neighbouring core locations. GeoB1515-1, recovered from 3,129 m and GeoB1523-1 from 3,292 m water depth from the eastern and south-western Ceara Rise, located 1,000 km and 800 km northeast from the Amazon River mouth, respectively and situated only ~240 km apart. Results for $^{231}Pa/^{230}Th$ and ε_{Nd} from both cores display a high level of coherency, testifying to the robustness of the methodological and analytical approach (Fig. 2c,d, supporting material S4). For ε_{Nd}, similar to the trends of Site 12JPC and the Bermuda Rise records, the Holocene and the glacial display distinct values ($\Delta\varepsilon_{Nd}$ =2-3), similar to the trends seen in $\delta^{13}C$ from epibenthic foraminifera (Mulitza et al., 1998). Most unradiogenic values in ε_{Nd} are not reached at the uppermost (youngest) samples, but during the mid-Holocene at these sites, as previously also reported for 12JPC (Gutjahr et al., 2008), the Bermuda Rise record (Roberts et al., 2010) and the Wyville-Thomson Ridge (ODP 980) (Crocket et al., 2011) (supporting material S1). Analogous to ε_{Nd} signatures, the $^{231}Pa/^{230}Th$ record shows values distinguishing the Holocene (average=0.056, n=6) from the peak glacial (average=0.071, n=4) and the deglacial (average=0.079, n=10) parts. In contrast to ε_{Nd} or the $^{231}Pa/^{230}Th$ record from 12JPC, highest $^{231}Pa/^{230}Th$ ratios are observed between 11 and 15 ka. There is some evidence of increased biogenic particle fluxes in GeoB1523-1 during this time period (Kasten et al., 2001), as well as higher opal concentrations in a number of equatorial sediment cores (Bradtmiller et al., 2007) in relative proximity to GeoB1515-1 and GeoB1523-1, which would be capable of increase the ^{231}Pa scavenging efficiency. But low concentrations of biogenic opal (< 3 %, see following section 3.6) at these sites argue against opal being a primary control on the sedimentary distribution of $^{231}Pa/^{230}Th$ (e.g. the highest opal concentration of GeoB1515-1 is measured at 24 ka when $^{231}Pa/^{230}Th$ was low). The available data sets cannot distinguish between a signal of weaker AMOC around the YD as found from the high resolution Bermuda Rise record (McManus et al., 2004) or higher particle fluxes induced by increased Amazon river outflow (Mosblech et al., 2012).

3.4 M35003-4

Core M35003-4 is the shallowest core of our compilation, retrieved from 1,299 m water depth. In comparison to the deeper cores its variability in both $^{231}Pa/^{230}Th$ and ε_{Nd} is substantially smaller, although the relatively low temporal resolution may mask some of the variability (Fig. 2e). The ε_{Nd} profile is in very good agreement with values from the neighbouring core MD99-2198 (Pahnke et al., 2008), but lower temporal data coverage does not allow resolving increased northward propagation of AAIW during HS1 or the YD as observed at site MD99-2198 (supporting material S1).

The $^{231}Pa/^{230}Th$ values are close to the production ratio and persistently higher compared to the deeper cores as a consequence of the shallow water-depth: In the Atlantic Ocean high circulation intensity above a specific location causes $^{231}Pa/^{230}Th$ to decrease with water depth because of the permanent advective ^{231}Pa export due to higher residence time in comparison to ^{230}Th. Along with enhanced scavenging of ^{231}Pa close to the surface the result is higher $^{231}Pa/^{230}Th$ in shallower waters than in deeper waters (Lippold et al., 2011; Luo et al., 2010). Thus, these high absolute values may not be interpreted directly as an indicator of weak circulation.

3.5 ODP Site 1089

The southernmost core site of this study, ODP Site 1089, is located in the south-eastern South Atlantic at the northern flank of the Agulhas Ridge in the southern Cape Basin at 4,621 m water depth. Today the site is situated at the interface of NADW and Circumpolar Deep Water (CDW) with a strong influence of Antarctic Bottom Water (AABW) (Govin et al., 2009).

Our ε_{Nd} record (Fig. 2f) corroborates the records from adjacent sites RC11-83 (Piotrowski et al., 2004) and MD07-3076 (Skinner et al., 2013) very well (supporting material S1). Due to its southern position the Holocene ε_{Nd} signatures are far more radiogenic than in the North- or Equatorial Atlantic, but clearly indicate a contribution of NADW featuring average Holocene values of -9.3. The temporal trend in ε_{Nd} mirrors the trends of the other deep cores with radiogenic glacial values and a subsequent gradual decrease of ε_{Nd} into the Holocene, but with a far later turning point than the other deeper cores. $^{231}Pa/^{230}Th$ at ODP Site 1089 equally develops from high glacial towards lower Holocene values.

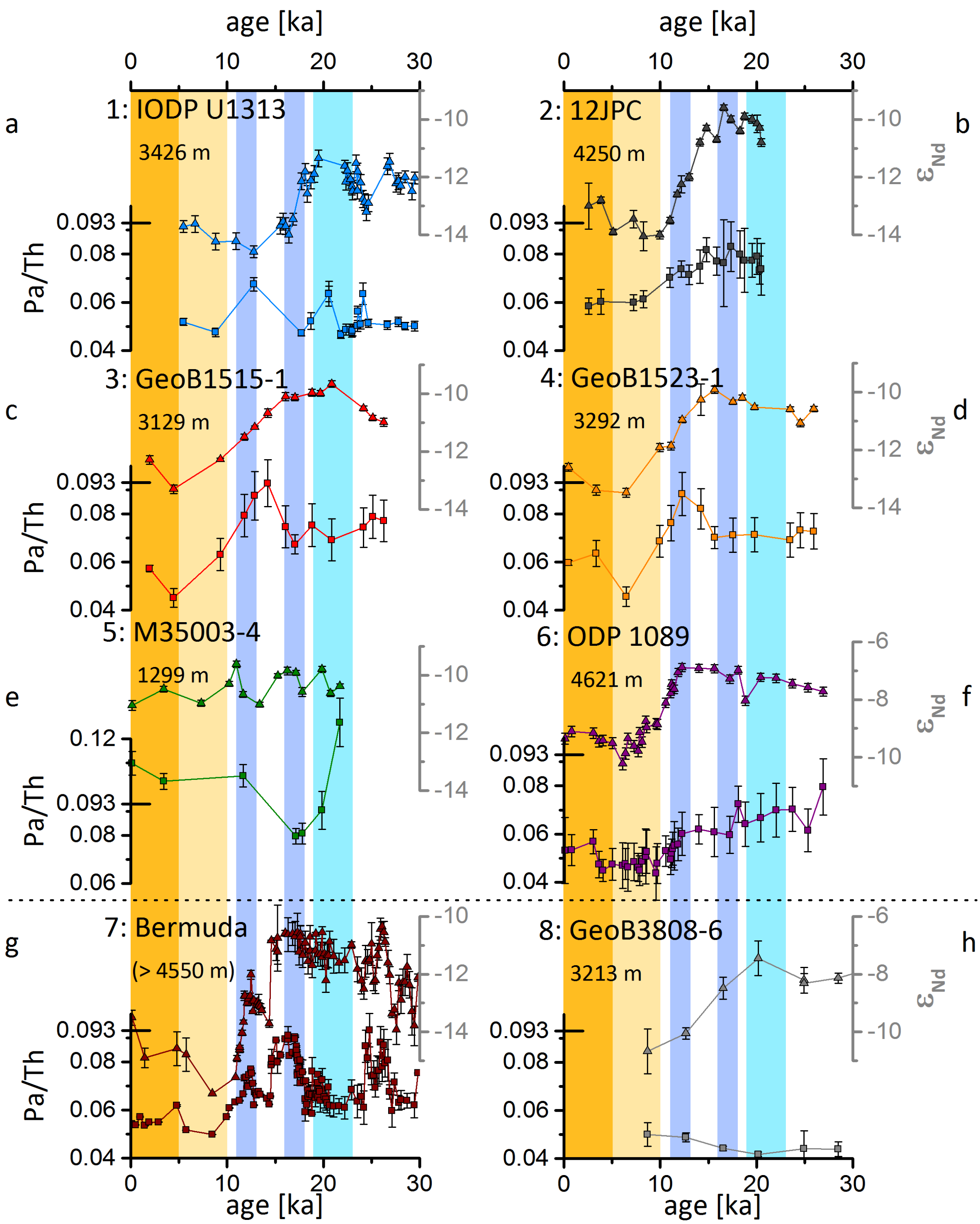

Fig. 2: (a-f) New combined $^{231}Pa/^{230}Th$ and ε_{Nd} records from six sediment cores located across the entire Atlantic basin extended by combined data sets from the literature below the dotted line (g: Bermuda Rise and h: South Atlantic GeoB3808-6:(Jonkers et al., 2015)). The Bermuda Rise record (g) is a combination of the $^{231}Pa/^{230}Th$ and ε_{Nd} profiles reported by (Gutjahr and Lippold, 2011; Lippold et al., 2009; McManus et al., 2004; Roberts et al., 2010). Y-axes ranges have been kept constant with exception of $^{231}Pa/^{230}Th$ at the shallowest core M35003-4 (e) and ε_{Nd} at the two southern cores ODP Site 1089 and GeoB3808-6 (f,h). Vertical bars indicate the time ranges of the LGM, Heinrich Stadial 1, Younger Dryas and the early and later Holocene.

3.6 Opal and ^{231}Pa/^{230}Th

As mentioned above, we examined whether variations in ^{231}Pa/^{230}Th were accompanied by corresponding variations in the sedimentary opal concentrations. In general no significant positive correlation (R^2=0.11, n=108) between ^{231}Pa/^{230}Th and opal can be found across all examined time periods and sediment cores (cross-plot in Fig. 3a and time-series in supplementary material S5) in agreement with recent measurements from water column samples from a cross-Atlantic transect (Hayes et al., 2015). As previously found by Rutberg et al. (2000) for deep seawater, on a basin-wide scale opal concentrations show a correlation with ε_{Nd} instead (Fig. 3b). This correlation is likely a result of opal preservation in SCW influenced sediment-water interfaces providing indirect evidence for the northward advances of SCW during the last glacial and the deglacial compared to the Holocene. Given the effect of enhanced opal-preservation in locations bathed by SCW and the lack of correlation between ^{231}Pa/^{230}Th and opal, increased ^{231}Pa/^{230}Th values during times of radiogenic ε_{Nd} most likely indicate changes in ocean circulation and not in particle composition. We hence consider variations in ^{231}Pa/^{230}Th from all sites, with the possible exception of the southernmost ODP Site 1089, as predominantly driven by circulation changes.

The opal concentrations from ODP 1089 vary in concert with ^{231}Pa/^{230}Th (supplementary material S5,) suggesting a possible influence of opal on the scavenging efficiency of ^{231}Pa (R^2=0.78, n=35). The location of ODP Site 1089 is very close to the southern opal belt. Given the coincident increase in both opal and ^{231}Pa/^{230}Th it seems plausible that a northward migration of the opal belt during the glacial (Asmus et al., 1999) may have influenced ^{231}Pa/^{230}Th. However, despite the clearly higher sedimentary opal content in core ODP1098, the ^{231}Pa/^{230}Th values are generally similar to the range of ^{231}Pa/^{230}Th values recorded in other locations spanning the Atlantic Ocean (Fig. 3a). Hence increased opal flux may have shifted ^{231}Pa/^{230}Th towards higher values, but ocean circulation still exerts the primary control over ^{231}Pa/^{230}Th at this location.

a

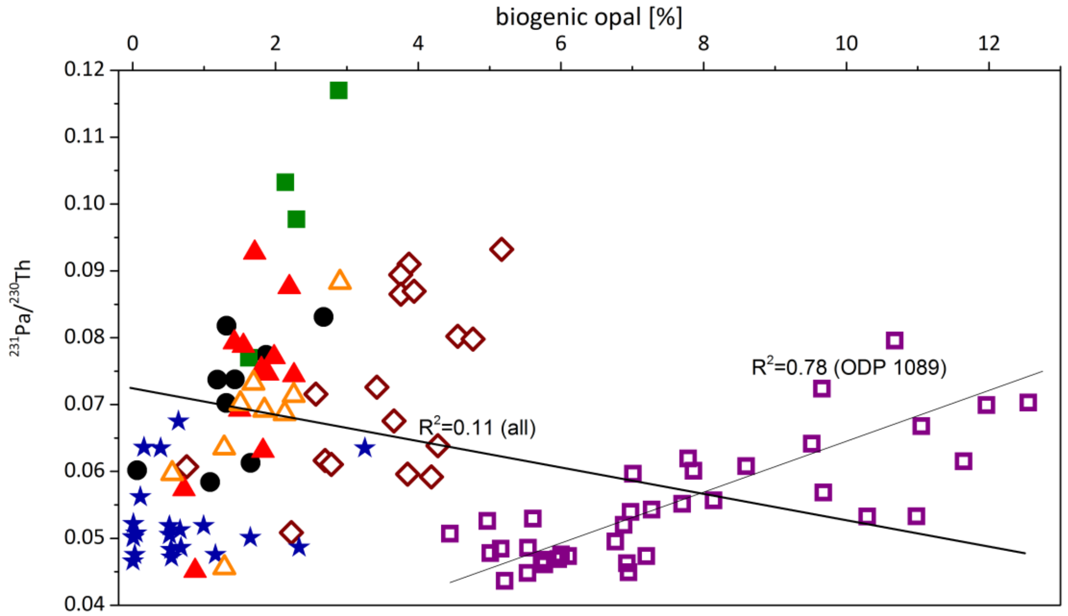

b

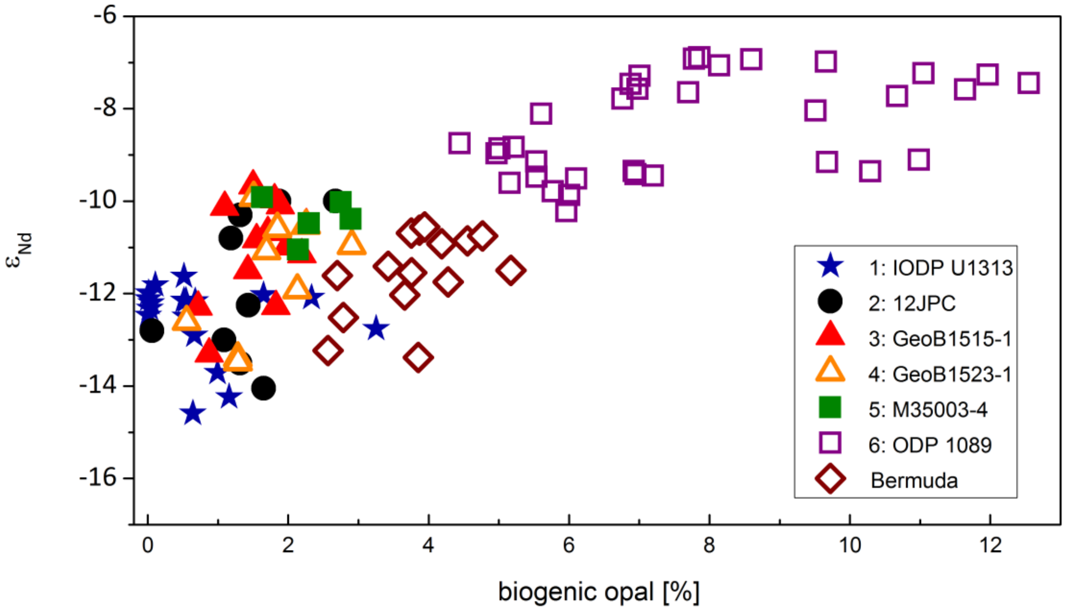

Fig. 3:
Opal concentrations versus a) $^{231}Pa/^{230}Th$ and b) ε_{Nd} for all available data pairs from this study and for the Bermuda Rise (ODP1063)(Böhm et al., 2015). The negative slope of the basin wide regression line does not suggest an influence of opal on $^{231}Pa/^{230}Th$ (a). Opal concentrations generally increase with stronger contributions from SCW as indicated by the correlation with ε_{Nd} (b).

3.7 Glacial-Holocene variations of water mass provenance indicated by ε_{Nd}

The Holocene distribution of authigenic ε_{Nd} robustly reflects the geometry of NCW and SCW in the modern Atlantic Ocean (Fig. 1b and S2). During the LGM a general shift toward more radiogenic values at all sites indicates increased influence of SCW over the entire glacial Atlantic (Fig. 4a). However, the magnitudes of the shifts in ε_{Nd} vary with the core location. Sediments in the western North Atlantic (12JPC, Fig. 2b; GeoB1515-1, Fig. 2c; GeoB1523-1, Fig. 2d; Bermuda Rise, Fig. 2g) undergo a shift of at least 2-3 $\Delta\varepsilon_{Nd}$. This is interpreted as reflecting a transition in the deep water mass regime, from glacial SCW to Holocene NCW bathing these sites (cf. (Gutjahr et al., 2008)). The smallest LGM-Holocene gradient is observed for the shallowest core M35003-4 ($\Delta\varepsilon_{Nd}$ = 0.6, Fig. 2e). The glacial-interglacial difference for M35003-4 is barely above the analytical uncertainties, implying a persistent presence of NCW and a sustained northern overturning cell during the LGM in the shallower North Atlantic (Lippold et al., 2012b). Although the northernmost core of this study, IODP Site U1313 (Fig. 2a), is located deeper than GeoB1515-1 and GeoB1523-1 (Fig. 2c,d), which are fully bathed by SCW during the LGM, ε_{Nd} at Site IODP Site U1313 never rises above -11.3 due to its more northern position. For comparison Bermuda Rise, 12JPC and Ceara Rise maxima during the LGM are -10.3, -9.6 and -9.7, respectively. Hence, the North Atlantic ε_{Nd} records imply a shoaling of the GNAIW/SCW interface towards the south during the LGM rather than a separation of SCW and GNAIW at a specific water depth (Gebbie, 2014).

The cores from the southern hemisphere also evidence a pronounced dominance of SCW during the glacial, indicated by radiogenic ε_{Nd} as suggested previously (Piotrowski et al., 2004). While the deep ODP Site 1089 (Fig. 2g) witnesses contributions from NCW today (ε_{Nd} = -9.3), it was barely influenced by contributions from NCW during the LGM (ε_{Nd} = -7.3). This effect is even more pronounced for the shallower site GeoB3808-6 (Fig. 2h, Holocene ε_{Nd} = -10.7, LGM ε_{Nd} = -7.5), which was completely isolated from any supply from NCW. The presence of SCW in the entire Atlantic lasted beyond the LGM at all core sites, indicated by relatively radiogenic SCW Nd isotope signatures at least until 17 ka (Fig. 2). For the ε_{Nd} down-core-profiles of the cores below 3,000 m water depth a distinct time can be identified after which values started to evolve towards more unradiogenic signatures. This change emerges first at the northernmost core IODP U1313 around 17 ka. Having already been influenced by the GNAIW overturning cell during the LGM, the ε_{Nd} signatures from this core reacted most readily to the incipient retreat of SCW. For 12JPC, GeoB1515-1, GeoB1523-1 and the Bermuda Rise cores the turning points were reached later (approximately 2 ka) at around the Bølling/Allerød warm period. For ODP1089 in the deep south-eastern Atlantic it took longest (around 12 ka BP) before a steady descent towards unradiogenic values was initiated. In contrast to an earlier appearance of this switch at other core locations in the South Atlantic (e.g. GeoB3808-6 and MD07-3076 (Skinner et al., 2013)), strong influence of NCW reached the deep South Atlantic at ODP1089, east of the Mid Ocean Ridge, several ka later. The gradual decrease of ε_{Nd} at all sites lasted around 5,000 years eventually reaching the least radiogenic values in the course of the Holocene with subsequent tendencies towards more radiogenic contributions afterwards. The deglacial evolution from a SCW dominated Atlantic towards a NCW regime did therefore not occur as a sudden switch from GNAIW to NADW, but instead was a progressive process, as also suggested from other $^{231}Pa/^{230}Th$ and ε_{Nd} based studies (Böhm et al., 2015; Skinner et al., 2013). This gradual substitution of SCW by NCW implies a slow deglacial evolution of the AMOC until maximum NCW domination was reached during the early Holocene.

Another time period of interest is HS1 (~15 to 18 ka). Within error the HS1 ε_{Nd} compositions were virtually identical to the LGM (Fig. 2). This is most likely a result of the fact that SCW already occupied most of the volume of the abyssal Atlantic during the LGM. Hence no significant changes in ε_{Nd} resulting from a potentially weaker contribution of NCW during HS1 can be observed (Fig. 4b). The only exception is IODP U1313 (Fig. 2a), which, due to its northernmost position, makes it more sensitive to the relative contributions of the NADW forming water masses (Iceland-Scotland Overflow Water, Denmark Strait Overflow Water, LSW). Variable rates of admixture of LSW at our core site may have produced more unradiogenic signatures towards the end of HS1 (Wilson et al. 2014), while the cores located to the southwest were still dominated by SCW (Figs. 3, 5b).

a

b

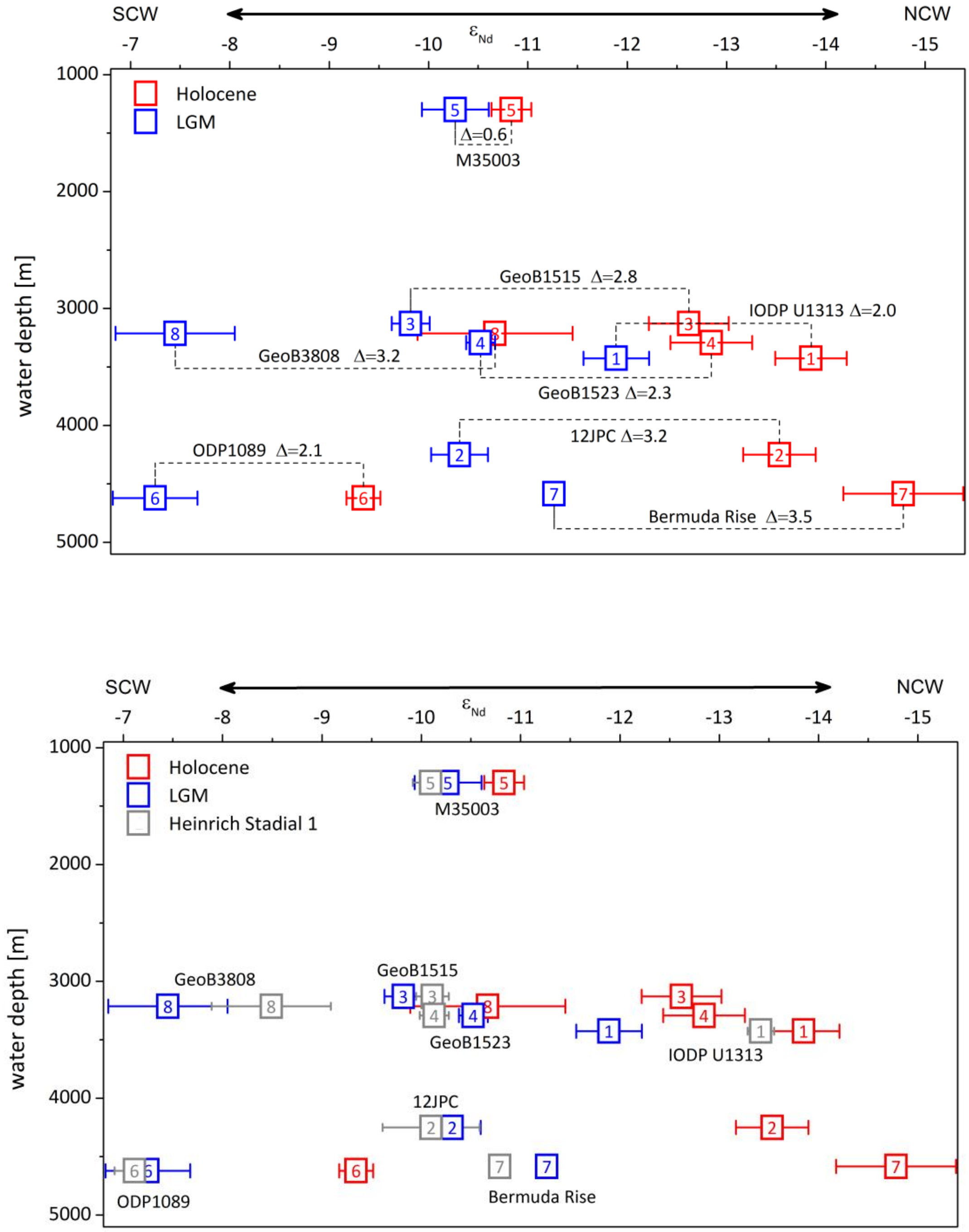

Fig. 4: Water depth versus

a) *ε_{Nd} for the time slices of the Holocene (averaged from 0-10 ka, red) and the LGM (averaged from 19-23 ka, blue). Dashed lines indicate the changes in ε_{Nd}. Numbers within the symbols refer to the individual cores (Table 1). Error bars give the standard error for the average of each time slice. If only one datum is within the limits of the time slice, the analytical external reproducibility is given.*

b) *ε_{Nd} of HS1 (averaged from 15-18 ka, grey) is added.*

3.8 Glacial-Holocene evolution of ocean circulation from a two-proxy point of view

The absolute values and trends in the $^{231}Pa/^{230}Th$ down-core records presented in this study (Fig. 2) confirm that information about past changes in AMOC strength should ideally be derived from a set of different core locations, both geographically and from various water depths. In conjunction with ε_{Nd} records, an even more comprehensive picture of the LGM water mass advection can be reconstructed.

Holocene $^{231}Pa/^{230}Th$ ratios, featuring values clearly below the production ratio, reflect active export of ^{231}Pa out of the Atlantic Ocean along with NADW (Fig. 5, red). A general deficit of ^{231}Pa is observed for the LGM (blue) as well, but significantly higher ratios for almost all locations imply less vigorous water mass advection, in particular in the deep ocean. The cores that have experienced significant glacial/interglacial changes in ε_{Nd} indicative of a change in the source of the water mass also display the most pronounced changes in $^{231}Pa/^{230}Th$ (GeoB1515-1, GeoB1523-1, 12JPC, Bermuda cores, ODP Site 1089). At this point it is important to note that the $^{231}Pa/^{230}Th$ of these deeper cores does not provide information about the strength of shallower GNAIW since the core sites were bathed by SCW, and because the predominant part of the $^{231}Pa/^{230}Th$ signal is generated within ~1 km above the sediment (Thomas et al., 2006). Instead during the LGM these deeper locations consistently indicate a weaker circulation (higher $^{231}Pa/^{230}Th$ compared to the Holocene) related to the SCW cell. Both proxies record the transition of a SCW dominated deep Atlantic Ocean to a NCW dominated North Atlantic from the onset of the deglaciation in good agreement with findings based on nutrient-based proxies such as benthic $\delta^{13}C$ and Cd/Ca (Gebbie, 2014). However, there are three cores characterised by unchanged (IODP U1313, M35003-4) or even lower (GeoB3808-6) $^{231}Pa/^{230}Th$ during the LGM (Fig. 5a). Such invariable $^{231}Pa/^{230}Th$ values stand in contrast to the varying ε_{Nd}-signatures at IODP Site U1313 and GeoB3808-6, which follow the general trend of more radiogenic values in the glacial and more unradiogenic values in the Holocene. The glacial decrease in $^{231}Pa/^{230}Th$ at GeoB3808-6 may be a consequence of a ^{231}Pa depletion of the water mass caused by the northward migration of the opal belt (Negre et al., 2010) (also indicated by the correlation of $^{231}Pa/^{230}Th$ with opal concentrations at ODP Site 1089). But more likely the deep South Atlantic may have become a source of ^{231}Pa for the deep North Atlantic due to the dominance of northward flowing SCW during the glacial, turning over the interglacial situation (Jonkers et al., 2015).

In the north ε_{Nd} at IODP Site U1313 equally indicates more radiogenic signatures during the glacial, but with more unradiogenic absolute values (LGM average ε_{Nd} ≈-12), which is indicative of significant NCW admixtures to glacial local deep water. Similarly, the shallowest core M35003-4 shows a barely resolvable shift towards more radiogenic signatures ($\Delta\varepsilon_{Nd}$=0.6). Since the water mass provenance signal and the circulation strength at IODP Site U1313 and M35003-4 changed far less than the deeper and more southerly cores, we conclude that there was still an active northern overturning cell of GNAIW during the LGM. Combining the above observations, we find support for a sluggishly ventilated, SCW-dominated deep Atlantic during the LGM as suggested by the distribution of $\delta^{13}C$ (Curry and Oppo, 2005; Sarnthein et al., 1994). Additionally, information about the strength and directions of deep water circulation is observed (Fig. 6). Still, as yet the spatial resolution does not allow distinguishing between the situation in the eastern and the western basins or for more specific water depths.

3.9 Heinrich Stadial 1

Heinrich Stadial 1 that followed the LGM featured no pronounced changes in $^{231}Pa/^{230}Th$ compared to the LGM for most of the locations, implying a still active NCW overturning cell during HS1 (Bradtmiller et al., 2014; Oppo et al., 2015). Lower HS1 values at ODP Site 1089 and higher values at the Bermuda Rise were accompanied by changes in opal concentrations (S5, (Keigwin and Boyle, 2008; Lippold et al., 2009)) and may not be solely explained by circulation changes. The largest change in $^{231}Pa/^{230}Th$ during HS1 compared to the Holocene or the LGM was observed for M35003-4 (Fig. 5b). The two lower values during HS1 may indicate an intensified GNAIW circulation cell. However, the low sampling resolution for this record prevents an unbiased interpretation during this time interval. There is an obvious need of higher temporal and spatial resolution to better constrain the structure of the upper branch of the past AMOC during HS1.

a

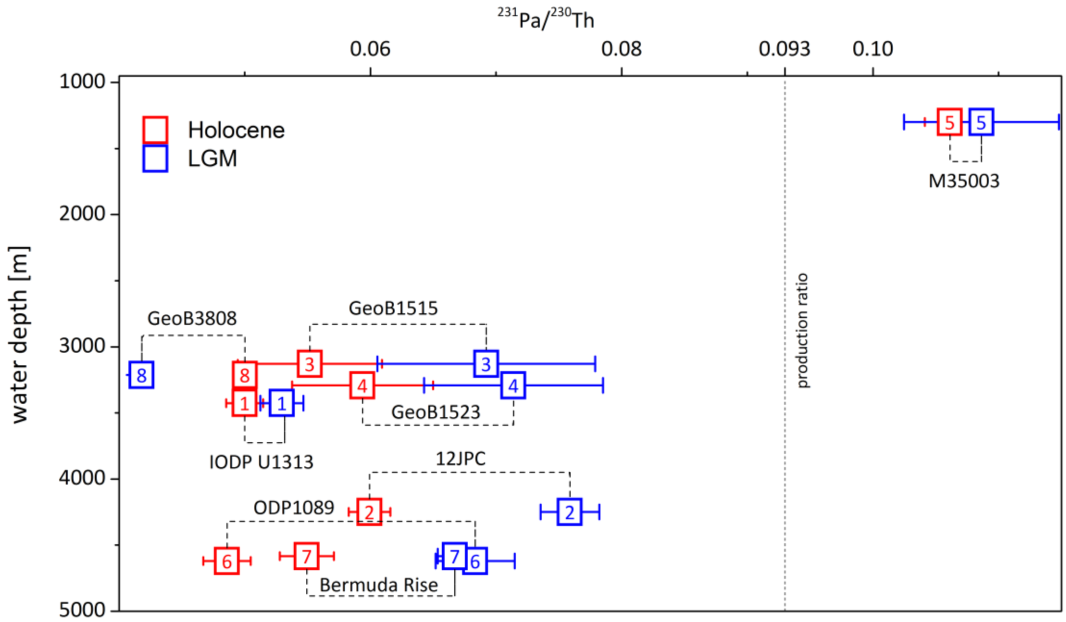

b

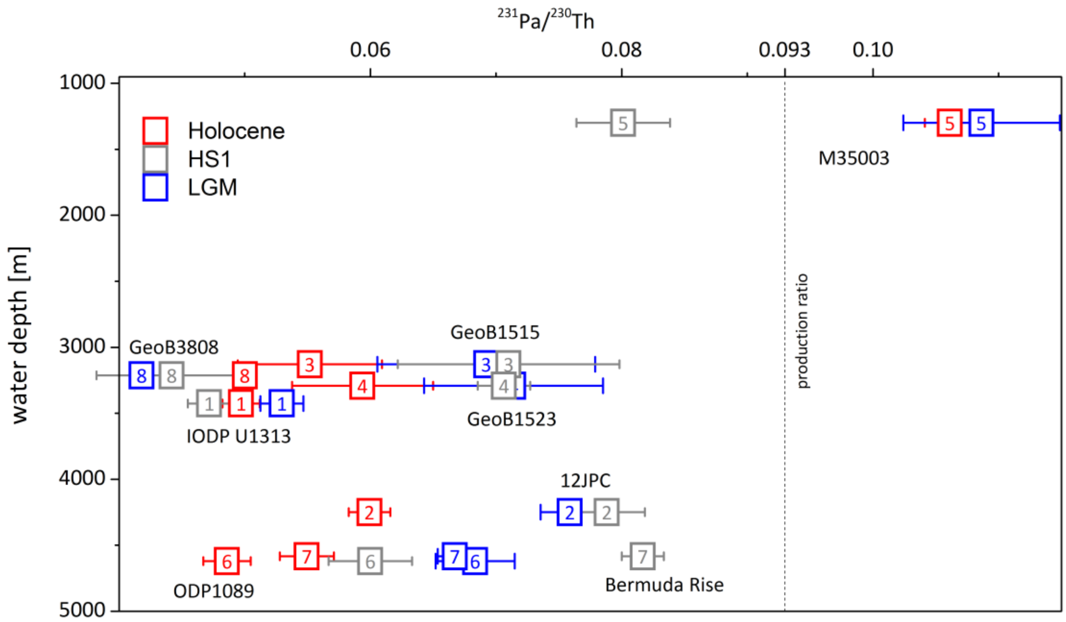

Fig. 5:

a) *Water depth versus $^{231}Pa/^{230}Th$ for the time slices of the Holocene (averaged from 0-10 ka, red) and the LGM (averaged from 19-23 ka, blue). Dashed lines indicate the changes in $^{231}Pa/^{230}Th$. Numbers within the symbols refer to the individual cores (Table 1). Error bars give the standard error for the average of each time slice. If only one datum is within the limits of the time slice, the analytical external reproducibility is given.*

b) *$^{231}Pa/^{230}Th$ averages of HS1 (averaged from 15-18 ka, grey) are added.*

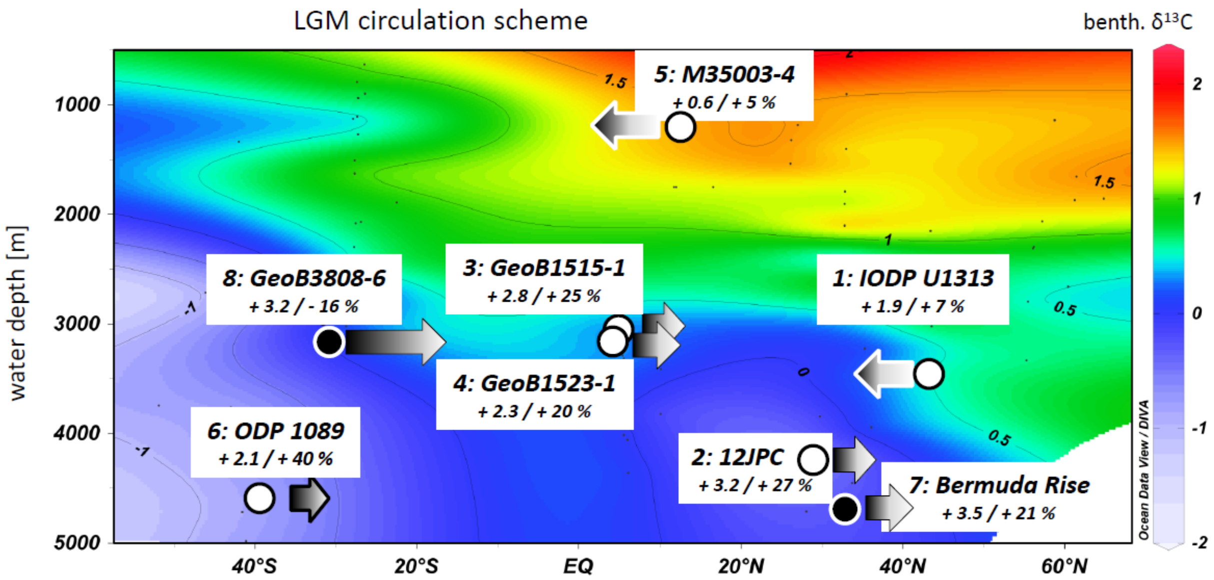

Fig. 6: LGM AMOC circulation scheme based on $^{231}Pa/^{230}Th$, ε_{Nd} and $\delta^{13}C$ (values indicated by contour lines and colour code (Curry and Oppo, 2005)) indicate a shoaled NCW overturning cell. Overlain on the $\delta^{13}C$ compilation are directions and relative advection strengths during the LGM derived from $^{231}Pa/^{230}Th$ and ε_{Nd} for each core location. Shadings of the arrows indicate the contribution of NCW (white) relative to SCW (black) according to a linear end-member mixing model. Lengths of the arrows are scaled to the relative changes in $^{231}Pa/^{230}Th$ between the LGM and the Holocene. Numbers underneath the core names indicate the differences in ε_{Nd} and relative increases in $^{231}Pa/^{230}Th$ values during the LGM compared to the average Holocene values.

3.10 Variability of the Holocene AMOC

Another noteworthy feature in the down-core profiles of both proxies is the sporadic appearance of lower values in $^{231}Pa/^{230}Th$ and/or ε_{Nd} for several of the cores (Fig. 2, and supporting material S1) in the early or mid- Holocene. More negative ε_{Nd} values alone may simply indicate an increased contribution of LSW to NADW. However, concurrent decreases in some of the $^{231}Pa/^{230}Th$ profiles point to a stronger contribution of NCW compared to the more recent time period of the Holocene. In this case such values may reflect an enhanced AMOC circulation mode (Thornalley et al., 2013) facilitating the basin-wide spreading of NADW at higher advection rates during distinct time intervals of the Holocene. The timing of the appearances of these low values in $^{231}Pa/^{230}Th$ and ε_{Nd} are however not always concordant: the minima in $^{231}Pa/^{230}Th$ and ε_{Nd} are observed not only at the onset of the Holocene, but also sometimes around the mid-Holocene (ODP Site 1089, IODP U1313), or the minima are observed for one proxy only (12JPC, IODP U1313). Consequently, the suggestion of an early Holocene AMOC overshoot needs further corroboration.

4 Conclusions

We observe no basin wide correlation of the $^{231}Pa/^{230}Th$ with the abundance of opal, with the exception of the southernmost core (ODP Site 1089). For all the northern locations the generally robust correlation of ε_{Nd} with opal concentrations suggests that opal is better preserved at core locations bathed by SCW. Hence, co-variation of $^{231}Pa/^{230}Th$ with opal does not necessarily indicate a causal link (i.e., high opal causes high $^{231}Pa/^{230}Th$) but instead results from a change in the water mass provenance.

The new data presented here spanning the entire Atlantic contribute to improving the spatial resolution of the past AMOC variability by applying two independent proxies, $^{231}Pa/^{230}Th$ and Nd isotopes. These proxies, unaffected by changes in the global carbon cycle, allow the reconstruction of circulation strength and deep water provenance.

Our basin wide analysis of the combined data sets of six new and two published $^{231}Pa/^{230}Th$ and ε_{Nd} records consistently suggest higher $^{231}Pa/^{230}Th$ and more radiogenic ε_{Nd} values during the LGM and HS1 compared with the Holocene. These results confirm the increased influence, as well as the northward advection, of sluggishly ventilated SCW deep waters during the LGM and HS1, followed by a subsequent change towards a NCW dominated and stronger ventilated North Atlantic, supporting the classical paleoceanographic point of view (Curry and Oppo, 2005; Sarnthein et al., 1994).

Exceptions to these general features are observable at the northernmost (IODP U1313) and shallowest (M35003-4) core locations of this study, evidencing the presence of NCW contributions (GNAIW) to prevailing SCW and an active shallow overturning cell during the LGM.

During the deglaciation both proxies indicate a gradual transition, lasting several millennia, towards a NCW dominated and stronger ventilated North Atlantic. The imprints of the reorganisation of the circulation pattern can be found earliest in the North (IODP U1313) at about 17 ka and arrives latest in the deep south-east Atlantic (ODP1089) at about 11 ka.

There are periods in the Holocene when $^{231}Pa/^{230}Th$ and/or ε_{Nd} from some of the new records indicate a more active AMOC than during the later Holocene, suggesting potential intra-Holocene variations in the AMOC. However, insufficient data coverage during the Holocene, and different timing of these peaks, do not allow a clear identification of an early Holocene AMOC overshoot and/or a mid-Holocene "Super-AMOC" mode.

5 Acknowledgements

This project was funded by DFG grant Li1815/2. J. Lippold was further supported by the FP7-PEOPLE-2013-IEF, Marie Curie proposal 622483. We thank the ODP core repository and the MARUM GeoB Core Repository in Bremen for dedicated support. Stefan Mulitza was supported through the DFG Research Center/Cluster of Excellence ''The Ocean in the Earth System''. E. Böhm acknowledges support from the European Research Council grant ACCLIMATE/no 339108. S.L. Jaccard and O. Cartapanis were supported by the Swiss National Science Foundation (grant PP00P2_144811). Chris Coath at the University of Bristol and Andy Milton at the University of Southampton are thanked for excellent machine support and Carsten Münker for access to the Neptune lab in Bonn. We thank Alexander Thomas and two anonymous reviewers for their constructive criticism and Derek Vance for very helpful editorial handling. Figure 1 was generated using the Ocean Data View software by Reiner Schlitzer.

6 References

1. Asmus, T., M. Frank, C. Kochschmieder, N. Frank, R. Gersonde, G. Kuhn, Mangini, A., 1999. Variations of biogenic particle flux in the southern Atlantic section of the Subantarctic zone during the late Quaternary: Evidence from sedimentary $^{231}Pa_{ex}$ and $^{230}Th_{ex}$. Marine Geology 159, 63-78.

2. Böhm, E., J. Lippold, M. Gutjahr, M. Frank, P. Blaser, B. Antz, J. Fohlmeister, N. Frank, M.B. Andersen, Deininger, M., 2015. Strong and deep Atlantic Meridional Overturning Circulation during the last glacial cycle. Nature 517, 73-76.

3. Bourne, M., A. Thomas, C. Niocaill, Henderson, G., 2012. Improved determination of marine sedimentation rates using $^{230}Th_{xs}$. Geochemistry Geophysics Geosystems 13, Q09017.

4. Bradtmiller, L., McManus, J.F., Robinson, L.F., 2014. $^{231}Pa/^{230}Th$ evidence for a weakened but persistent Atlantic meridional overturning circulation during Heinrich Stadial 1. Nature Communications 5, 5817.

5. Bradtmiller, L., R. Anderson, M. Fleisher, Burckle, L., 2007. Opal burial in the equatorial Atlantic Ocean over the last 30 kyr: implications for glacial-interglacial changes in the ocean silicon cycle. Paleoceanography 22, PA4216.

6. Channell, J., T. Sato, T. Kanamatsu, R. Stein, C. Alvarez Zarikian, and the Expedition 303/306 Scientists, 2006. Expedition 303/306 synthesis: North Atlantic climate Proc. IODP, 303/306. College Station, TX (IODP Management International).

7. Chase, Z., R. Anderson, M. Fleisher, Kubik, P., 2002. The influence of particle composition and particle flux on scavenging of Th, Pa and Be in the ocean. Earth and Planetary Science Letters 204, 215-229.

8. Christl, M., J. Lippold, A. Hofmann, L. Wacker, Y. Lahaye, Synal, H., 2010. $^{231}Pa/^{230}Th$: a proxy for upwelling off the coast of West Africa. Nuclear Instruments and Methods in Physics Research B 268, 1159–1162.

9. Christl, M., Wacker, L., Lippold, J., Suter, M., 2007. Protactinium-231, a new radionuclide for AMS. Nuclear Instruments and Methods in Physics Research B 262, 379–384.

10. Colin, C., N. Frank, K. Copard, Douville, E., 2010. Neodymium isotopic composition of deep-sea corals from the NE Atlantic: implications for past hydrological changes during the Holocene. Quaternary Science Reviews 29, 2509-2517.

11. Crocket, K., D. Vance, M. Gutjahr, G. Foster, Richards, D., 2011. Persistent Nordic deep water overflow to the glacial North Atlantic. Geology 39, 515-518.

12. Curry, W., Oppo, D., 2005. Glacial water mass geometry and the distribution of $d^{13}C$ of CO_2 in the western Atlantic Ocean. Paleoceanography 20, PA1017.

13. Elmore, A., A. Piotrowski, J. Wright, Scrivner, A., 2011. Testing the extraction of past seawater Nd isotopic composition from North Atlantic deep sea sediments and foraminifera. Geochemistry Geophysics Geosystems 12, Q09008.

14. Frank, M., 2002. Radiogenic isotopes: Tracers of past Ocean Circulation and erosional input. Reviews of Geophysics 40, 1001.

15. Galbraith, E., E. Kwon, D. Bianchi, M. Hain, Sarmiento, J., 2015. The impact of atmospheric pCO_2 on carbon isotope ratios of the atmosphere and ocean. Global Biogeochemical Cycles 29, 307–324.

16. Gebbie, G., 2014. How much did Glacial North Atlantic Water shoal? Paleoceanography 29, 190-209.

17. Geibert, W., Vöge, I., 2008. Progress in determination of 227-Ac in sea water. Marine Chemistry 109, 238-249.

18. Gherardi, J., L. Labeyrie, S. Nave, R. Francois, J. McManus, Cortijo, E., 2009. Glacial-interglacial circulation changes inferred from $^{231}Pa/^{230}Th$ sedimentary record in the North Atlantic region. Paleoceanography 24, PA2204.

19. Govin, A., Elisabeth Michel, Laurent Labeyrie, Waelbroeck, C., 2009. Evidence for northward expansion of Antarctic Bottom Water mass in the Southern Ocean during the last glacial inception. Paleoceanography 24, PA1202.

20. Gutjahr, M., Lippold, J., 2011. Early arrival of Southern Source Water in the deep North Atlantic prior to Heinrich event 2. Paleoceanography 26, PA2101.

21. Gutjahr, M., M. Frank, C. Stirling, L. Keigwin, Halliday, A., 2008. Tracing the Nd isotope evolution of North Atlantic Deep and Intermediate Waters in the western North Atlantic since the LGM from Blake Ridge sediments. Earth and Planetary Science Letters 266, 61–77.

22. Gutjahr, M., M. Frank, C. Stirling, V. Klemm, T. van de Flierdt, Halliday, A., 2007. Reliable extraction of a deepwater trace metal isotope signal from Fe–Mn oxyhydroxide coatings of marine sediments. Chem Geol 242, 351–370.

23. Hayes, C., Anderson, R.F., Fleisher, M.Q., Vivancos, S.M., Lam, P.J., Ohnemus, D.C., Huang, K.-F., Robinson, L.F., Lu, Y., Cheng, H., Edwards, R.L., Moran, S.B., 2015. Intensity of Th and Pa scavenging partitioned by particle chemistry in the North Atlantic Ocean. Marine Chemistry 170, 49-60.

24. Jaccard, S.L., Galbraith, E.D., Martínez-García, A., Anderson, R.F., 2016. Covariation of deep Southern Ocean oxygenation and atmospheric CO2 through the last ice age. Nature 530, 207-210.

25. Jeandel, C., 1993. Concentration and isotopic composition of neodymium in the South Atlantic Ocean. Earth and Planetary Science Letters 117, 581-591.

26. Jonkers, L., Zahn, R., Thomas, A., Henderson, G., Abouchami, W., François, R., Masque, P., Hall, I.R., Bickert, T., 2015. Deep circulation changes in the central South Atlantic during the past 145 kyrs reflected in a combined ^{231}Pa/^{230}Th, Neodymium isotope and benthic record. Earth and Planetary Science Letters 419, 14-21.

27. Kasten, S., R. Haese, M. Zabel, C. Rühlemann, Schulz, H., 2001. Barium peaks at glacial terminations in sediments of the equatorial Atlantic Ocean-relicts of deglacial productivity pulses? Chem Geol 175, 635–651.

28. Keigwin, D., Boyle, E., 2008. Did North Atlantic overturning halt 17,000 years ago? Paleoceanography 23, PA1101.

29. Keigwin, L., 2004. Radiocarbon and stable isotope constraints on Last Glacial Maximum and Younger Dryas ventilation in the western North Atlantic. Paleoceanography PA4012.

30. Kretschmer, S., W. Geibert, C. Schnabel, M. Rutgers van der Loeff, Mollenhauer, G., 2008. Distribution of ^{230}Th, ^{10}Be and ^{231}Pa in Sediment Particle Classes. Geochimica et Cosmochimica Acta 72.

31. Lacan, F., Jeandel, C., 2005a. Acquisition of the neodymium isotopic composition of the North Atlantic Deep Water. Geochemistry Geophysics Geosystems 6, Q12008.

32. Lacan, F., Jeandel, C., 2005b. Neodymium isotopes as a new tool for quantifying exchange fluxes at the continent - ocean interface. Earth and Planetary Science Letters 232, 245-257.

33. Lambelet, M., van de Flierdt, T., Crocket, K., Rehkämper, M., Kreissig, K., Coles, B., Rijkenberg, M.J.A., Gerringa, L.J.A., de Baar, H.J.W., Steinfeldt, R., 2015. Neodymium isotopic composition and concentration in the western North Atlantic Ocean: results from the GEOTRACES GA02 section. Geochimica et Cosmochimica Acta 177, 1-29.

34. Lippold, J., J. Gherardi, Luo, Y., 2011. Testing the ^{231}Pa/^{230}Th paleocirculation proxy - A data versus 2D model comparison. Geophysical Research Letters 38, L20603.

35. Lippold, J., J. Grützner, D. Winter, Y. Lahaye, A. Mangini, Christl, M., 2009. Does sedimentary ^{231}Pa/^{230}Th from the Bermuda Rise monitor past Atlantic Meridional Overturning Circulation? Geophysical Research Letters 36, L12601.

36. Lippold, J., S. Mulitza, G. Mollenhauer, S. Weyer, Christl, M., 2012a. Boundary scavenging at the east Atlantic margin does not negate use of Pa/Th to trace Atlantic overturning. Earth and Planetary Science Letters 333–334, 317-331.

37. Lippold, J., Y. Luo, R. Francois, S. Allen, J. Gherardi, S. Pichat, B. Hickey, Schulz, H., 2012b. Strength and geometry of the glacial Atlantic Meridional Overturning Circulation. Nature Geoscience 5, 813-816.

38. Luo, Y., R. Francois, Allen, S., 2010. Sediment ^{231}Pa/^{230}Th as a recorder of the rate of the Atlantic meridional overturning circulation: insights from a 2-D model. Ocean Science 6, 381-400.

39. Lynch-Stieglitz, J., Fairbanks, R.G., 1994. A conservative tracer for glacial ocean circulation from carbon isotope and palaeo-nutrient measurements in benthic foraminifera. Nature 369, 308-310.

40. McManus, J., R. Francois, J. Gherardi, L. Keigwin, Brown-Leger, S., 2004. Collapse and rapid resumption of Atlantic meridional circulation linked to deglacial climate change. Nature 428, 834-837.

41. Mosblech, N.A.S., Bush, M.B., Gosling, W.D., Hodell, D., Thomas, L., van Calsteren, P., Correa-Metrio, A., Valencia, B.G., Curtis, J., van Woesik, R., 2012. North Atlantic forcing of Amazonian precipitation during the last ice age. Nature Geoscience 5, 817-820.

42. Mulitza, S., C. Rühlemann, T. Bickert, W. Hale, J. Pätzold, Wefer, G., 1998. Late Quaternary d^{13}C gradients and carbonate accumulation in the western equatorial Atlantic. Earth and Planetary Science Letters 155, 237-249.

43. Negre, C., R. Zahn, A. Thomas, P. Masque, G. Henderson, G. Martinez-Mendez, I. Hall, Mas, J., 2010. Reversed flow of Atlantic deepwater during the Last Glacial Maximum. Nature 468, 84 - 89.

44. Oppo, D., W. Curry, McManus, J., 2015. What do benthic δ^{13}C and δ^{18}O data tell us about Atlantic circulation during Heinrich Stadial 1? Paleoceanography 30, 353–368.

45. Osborne, A.H., Haley, B.A., Hathorne, E.C., Flögel, S., Frank, M., 2014. Neodymium isotopes and concentrations in Caribbean seawater: Tracing water mass mixing and continental input in a semi-enclosed ocean basin. Earth and Planetary Science Letters 406, 174-186.

46. Pahnke, K., Goldstein, S., Hemming, S., 2008. Abrupt changes in Antarctic Intermediate Water circulation over the past 25,000 years. Nature Geoscience 1, 870-874.

47. Piepgras, D., Wasserburg, G., 1987. Rare earth element transport in the western North Atlantic inferred from Nd isotopic observations. Geochimica et Cosmochimica Acta 51, 1257-1271.

48. Piotrowski, A., S. Goldstein, S. Hemming, R. Fairbanks, 2004. Intensification and variability of ocean thermohaline circulation through the last deglaciation. Earth and Planetary Science Letters 225, 205-220.

49. Roberts, N., A. Piotrowski, J. McManus, Keigwin, L., 2010. Synchronous Deglacial Overturning and Water Mass Source Changes. Science 327, 75-78.

50. Rutberg, R., Sidney R. Hemming, Goldstein, S.L., 2000. Reduced North Atlantic Deep Water flux to the glacial Southern Ocean inferred from neodymium isotope ratios. Nature 405.

51. Sabine, C.L., Feely, R.A., Gruber, N., Key, R.M., Lee, K., Bullister, J.L., Wanninkhof, R., Wong, C.S., Wallace, D.W.R., Tilbrook, B., Millero, F.J., Peng, T.-H., Kozyr, A., Ono, T., Rios, A.F., 2004. The Oceanic Sink for Anthropogenic CO_2. Science 305, 367-371.

52. Sarnthein, M., K. Winn, S. Jung, J. Duplessy, L. Labeyrie, H. Erlenkeuser, Ganssen, G., 1994. Changes in east Atlantic deepwater circulation over the last 30,000 years: Eight time slice reconstructions. Paleoceanography 9, 209-267.

53. Scholten, J., J. Fietzke, A. Mangini, D. Garbe-Schönberg, A. Eisenhauer, P. Stoffers, Schneider, R., 2008. Advection and Scavenging: Effect on ^{230}Th and ^{231}Pa distribution off Southwest-Africa. Earth and Planetary Science Letters 271, 159-169.

54. Skinner, L.C., Scrivner, A.E., Vance, D., Barker, S., Fallon, S., Waelbroeck, C., 2013. North Atlantic versus Southern Ocean contributions to a deglacial surge in deep ocean ventilation. Geology 41, G34133.34131.

55. Tanaka, T., S. Togashi, H. Kamioka, H. Amakawa, H. Kagami, T. Hamamoto, M. Yuhara, Y. Orihashi, S. Yoneda, H. Shimizu, T. Kunimaru, K. Takahashi, T. Yanagi, T. Nakano, H.

Fujimaki, R. Shinjo, Y. Asahara, M. Tanimizu, Dragusanu, C., 2000. JNdi-1: a neodymium isotopic reference in consistency with La Jolla neodymium. Chem Geol 168, 279–281.

56. Thomas, A., G. Henderson, Robinson, L., 2006. Interpretation of the ^{231}Pa/^{230}Th paleocirculation proxy: New water-column measurements from the southwest Indian Ocean. Earth and Planetary Science Letters 241 493– 504.

57. Thornalley, D.J.R., Blaschek, M., Davies, F.J., Praetorius, S., Oppo, D.W., McManus, J.F., Hall, I.R., Kleiven, H., Renssen, H., McCave, I.N., 2013. Long-term variations in Iceland–Scotland overflow strength during the Holocene. Climate of the Past 9, 2073-2084.

58. Vance, D., Thirlwall, M., 2002. An assessment of mass discrimination in MC-ICPMS using Nd isotopes. Chem Geol 185, 227– 240.

59. Vidal, L., Schneider, R.R., Marchal, O., Bickert, T., 1999. Link between the North and South Atlantic during the Heinrich events of the last glacial period. Climate Dynamics 15, 909-919.

60. Wilson, D., Crocket, K.C., van de Flierdt, T., Robinson, L.F., Adkins, J.F., 2014. Dynamic intermediate ocean circulation in the North Atlantic during Heinrich Stadial 1: A radiocarbon and neodymium isotope perspective. Paleoceanography 29, PA002674.